Simple Model Representation of Atmosphere–Ocean GCMs and Estimation of the Time Scale of CO_2-Induced Climate Change

MICHAEL E. SCHLESINGER AND XINGJIAN JIANG

Department of Atmospheric Sciences, University of Illinois at Urbana-Champaign, Urbana, Illinois

(Manuscript received 23 June 1989, in final form 1 May 1990)

ABSTRACT

A simple atmosphere–ocean model is developed to represent the 20-year $1 \times CO_2$ and $2 \times CO_2$ simulations obtained with a coupled atmosphere–ocean general circulation model for the purpose of obtaining a new estimate of the characteristic response time of the climate system that accounts for oceanic upwelling.

The simple atmosphere–generalized ocean model consists of a zonally averaged energy balance climate model and a zonally averaged multilayer ocean model. The high latitudes of both hemispheres are combined into a single polar region, and the low and middle latitudes into a single nonpolar region. The atmosphere is treated as a single layer and the ocean as an arbitrary number of layers. The simple model includes the meridional transport of heat between the nonpolar and polar regions for both the atmosphere and each ocean layer. The ocean model includes the vertical advective heat transfer by the vertical velocity, the latter of which is prescribed and can vary with depth in both the polar and nonpolar regions. The unknown parameters of the simple model are the meridional heat fluxes between the nonpolar and polar regions, the coefficients of heat transfer within the ocean, the heat transfer coefficient between the ocean and atmosphere, an additional ocean–atmosphere heat transfer parameter, and the climate sensitivity parameter.

The parameters of the simple model are determined from the $1 \times CO_2$ and $2 \times CO_2$ simulations of the coupled atmosphere–ocean general circulation model. The simple atmosphere–ocean model is then used to project the response of the coupled atmosphere–ocean GCM from year 20 to year 100, and the resulting $2 \times CO_2 - 1 \times CO_2$ differences are normalized by the estimated equilibrium temperature changes. From these projections it is estimated that the characteristic response time is between 40 and 60 years, in close agreement with the estimates of Schlesinger et al.

1. Introduction

Observations show that the global-mean surface air temperature of the earth has increased by about 0.6°C from 1850 to 1980 (Jones et al. 1986; Hansen and Lebedeff 1987, 1988). It has been speculated that this rise in temperature represents the warming induced by increases in the concentrations of greenhouse gases in the earth's atmosphere, in particular, CO_2, CH_4, CFCs and N_2O. However, estimates of the expected greenhouse-gas-induced warming from 1850 to 1980, based on simulations by atmospheric general circulation/mixed-layer ocean models of the equilibrium temperature change induced by a CO_2 doubling, yield a value that is about twice as large as the observed warming over this time period (Schlesinger 1989). One possible explanation for this discrepancy is that our climate models are twice as sensitive as nature. Another explanation is that the climate system is not in equilibrium with the greenhouse gases due to the thermal inertia of the ocean.

Corresponding author address: Prof. Michael E. Schlesinger, Department of Atmospheric Sciences, University of Illinois, 105 South Gregory Avenue, Urbana, IL 61801.

Estimates of the time delay due to the ocean have been made with a variety of simplified atmosphere–ocean models with results that range from about 10 to 100 years for the characteristic e-folding time τ_e of the climate system (Hoffert et al. 1980; Bryan et al. 1982; Hansen et al. 1984; Bryan et al. 1984; Schlesinger et al. 1985; Bryan and Spelman 1985), defined as the time required for the evolving temperature change to reach 63% of the equilibrium temperature change. If τ_e is only 10 years, then the climate system is very close to being in equilibrium with the instantaneous greenhouse gas concentrations, and the discrepancy between the observed and model-predicted warmings would mean that our climate models are twice as sensitive as nature. However, if τ_e is as large as 100 years, then the discrepancy between the observed and model predicted warmings can be explained as being due to the reduction in the surface warming as a result of the downward transport of heat into the ocean. To obtain an accurate estimate of τ_e, however, requires a physically based model of the atmosphere–ocean system; that is, a global atmosphere–ocean General Circulation Model (GCM) in which the annual cycle of solar insolation is included.

Schlesinger et al. (1985) used such a coupled atmosphere–ocean general circulation model to esti-

mate the characteristic response time of the climate system to increases in atmospheric greenhouse gases. In particular, two 20 year simulations were performed, a $1 \times CO_2$ simulation with a CO_2 concentration of 326 ppmv, and a $2 \times CO_2$ simulation with the CO_2 concentration doubled. These simulations were not of sufficient duration to achieve equilibrium, a result which was anticipated. Consequently, to estimate τ_e, Schlesinger et al. (1985) used an energy-balance climate/box-diffusion ocean model in which the climate sensitivity and the oceanic diffusivity as a function of depth were parameters. These parameters were determined from the 20 year $1 \times CO_2$ and $2 \times CO_2$ simulations of the coupled atmosphere–ocean GCM. The resulting calibrated simple atmosphere–ocean model was then used to estimate the equilibrium warming and to project the evolution of the warming for 200 years. This evolving temperature change was then normalized by the equilibrium temperature change so that τ_e could be estimated. The resultant value of τ_e was found to be about 50 years for the surface air temperature and 75 years for the temperature of the upper layer of the ocean.

Harvey (1986) criticized the analysis of Schlesinger et al. (1985) on the grounds that their box-diffusion ocean model excluded upwelling and, thereby, yielded an overestimate for τ_e. Harvey (1986) argued that τ_e was overestimated because the equilibrium temperature changes of the atmosphere and the upper ocean layer were assumed to be identical, and because the transient response of the box-diffusion model can be very different from that of an ocean model that includes upwelling. Using such an upwelling-diffusion ocean model as an "analog" model to the ocean model of Schlesinger et al. (1985), Harvey (1986) found a value of τ_e equal to 27 years. Using the box-diffusion model, Harvey (1986) found that τ_e was 62 years for the atmosphere and 73 years for the upper ocean layer. Harvey (1986) concluded that Schlesinger et al. (1985) "appear to have overestimated values of τ_e for their long-term A/O GCM."

The analog model results of Harvey (1986), however, were obtained with an upwelling-diffusion ocean model for which the upwelling velocity was taken to be 47.4 m yr^{-1}, a value which is more than ten times the value of 4 m yr^{-1} generally used in such models (Hoffert et al. 1980). Consequently, it is not surprising that the value of τ_e estimated by Harvey (1986) is less than that obtained by Schlesinger et al. (1985) despite Harvey's use of diffusivities that were 2.2 times larger than those obtained by Schlesinger et al. (1985). Nevertheless, the criticism by Harvey (1986) of the analysis of Schlesinger et al. (1985) merits further consideration. Therefore, in this paper we remove the objections by Harvey (1986) of our previous analysis; first by developing a more general model of the ocean that includes upwelling, and second by using this generalized ocean model with realistic upwelling velocities to obtain new estimates of τ_e.

In section 2 we present our simple atmosphere-generalized ocean model and describe how its parameters are determined from the 20 year $1 \times CO_2$ and $2 \times CO_2$ simulations of the coupled atmosphere–ocean GCM. Section 3 then presents the results thereby obtained for the parameters of the simple model, discusses the method of closure of the model, and validates the resultant model against the results of the coupled GCM. The simple atmosphere–ocean model is then used to determine τ_e in section 4. Lastly, a summary is presented in section 5.

2. Representation of the $1 \times CO_2$ and $2 \times CO_2$ Simulations

a. *The model*

To represent the $1 \times CO_2$ and $2 \times CO_2$ results simulated by the OSU (Oregon State University) coupled atmosphere–ocean GCM, we will use the model shown schematically in Fig. 1. This model is a generalization

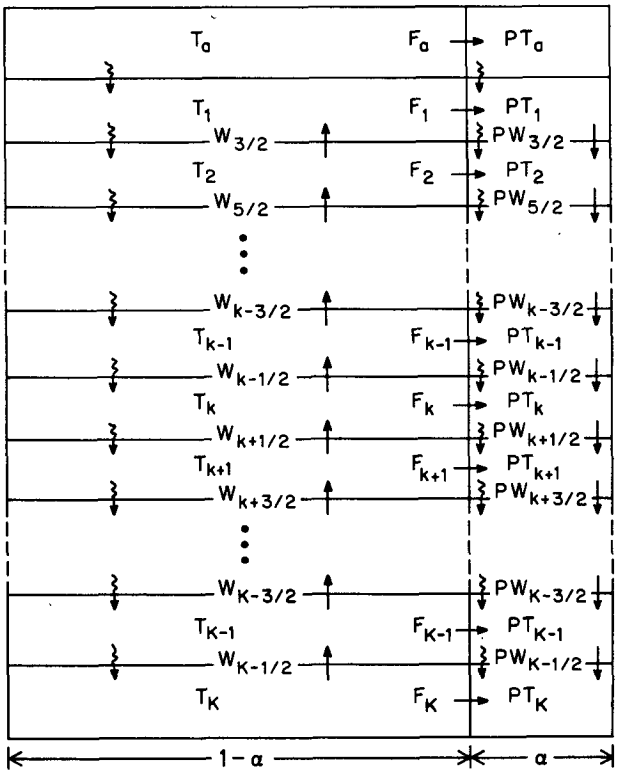

FIG. 1. Schematic representation of the simple atmosphere–ocean model. Here, T_a and PT_a are the temperatures of the atmosphere in the nonpolar and polar regions, respectively; T_k and PT_k are the corresponding temperatures of ocean layers $k = 1, \cdots, K$; $W_{k-1/2}$ and $PW_{k-1/2}$ for $k = 2, \cdots, K$ are the vertical velocities of the ocean in the nonpolar and polar regions, respectively, both positive upward; F_a and F_k for $k = 1, \cdots, K$ are the meridional heat transports from the nonpolar to the polar region in the atmosphere and ocean, respectively, and α is the fraction of the ocean occupied by the polar region.

of that of Hoffert et al. (1980) and consists of a zonally averaged energy-balance climate model and a zonally averaged multilayer ocean model. In each of these component models the high latitudes of both hemispheres are combined into a single polar region, and the low and middle latitudes of both hemispheres are combined into a single nonpolar region. In the model the atmosphere is treated as a single layer, with a horizontal area of unity, whose temperatures in the nonpolar and polar regions are T_a and PT_a, respectively. The ocean in the model is subdivided vertically into K layers, with each layer $k = 1, \cdots, K$ having a thickness $\Delta_k z$ and a horizontal area $(\sigma_{k+1/2})^{-1}$ relative to the area of layer $k + 1$. The nonpolar and polar regions of each ocean layer, respectively, occupy fractions $1 - \alpha$ and α of the horizontal area of the layer, and the temperatures of the nonpolar and polar regions are T_k and PT_k, respectively.

The energy-balance equation for the atmosphere in the nonpolar and polar regions can be written as

$$C_a \frac{\partial T_a}{\partial t} = Q - \lambda T_a - \sigma_a[A + \lambda_{a,o}(\mu T_a - T_1)] - \frac{F_a}{1 - \alpha} \quad (1)$$

and

$$C_a \frac{\partial PT_a}{\partial t} = Q - \lambda PT_a - \sigma_a[A + \lambda_{a,o}(\mu PT_a - PT_1)] + \frac{F_a}{\alpha}. \quad (2)$$

These equations state that the temperature of the atmosphere with heat capacity C_a changes in time t as a result of the heating by solar and longwave radiation, the heat exchange with the ocean, and the meridional heat transport between the nonpolar and polar regions. The heating by longwave radiation depends on the temperature, both directly through the Stefan-Boltzmann law and indirectly through the feedbacks of the climatic system. The longwave heating is represented here by a linearization about the longwave heating for a reference atmospheric temperature. The resultant reference longwave heating is then combined with the solar heating to give the term Q. The temperature-dependent part of the longwave heating is given by the terms λT_a and λPT_a, where λ characterizes the temperature sensitivity of the climatic system. The atmospheric heat exchange with the ocean is also linearized and the resultant reference heating is given by the term A. The temperature-dependent part of this heating is given by the terms $\lambda_{a,o}(\mu T_a - T_1)$ and $\lambda_{a,o}(\mu PT_a - PT_1)$, where $\lambda_{a,o}$ is an air–sea heat transfer coefficient and μ is a parameter that results from the fact that the longwave emissivity and relative humidity of the atmosphere may be less than unity. (The linearized equations are derived in the Appendix.) In Eqs. (1) and (2), σ_a multiplies the air–sea heat exchange terms to account for the difference between the area of the atmosphere (unity) and the area of the top layer of the ocean (σ_a). The last term in Eqs. (1) and (2) represents the heat exchange between the nonpolar and polar regions, with F_a being the meridional heat flux per unit horizontal area of the atmosphere.

The energy equations for the top layer of the ocean in the nonpolar and polar regions are

$$C_1 \frac{\partial T_1}{\partial t} = A + \lambda_{a,o}(\mu T_a - T_1) - \sigma_{3/2}\left[\lambda_{3/2}(T_1 - T_2) - \rho c W_{3/2} \frac{T_1 + T_2}{2}\right] - \frac{F_1}{1 - \alpha} \quad (3)$$

and

$$C_1 \frac{\partial PT_1}{\partial t} = A + \lambda_{a,o}(\mu PT_a - PT_1) - \sigma_{3/2}\left[\lambda'_{3/2}(PT_1 - PT_2) - \rho c PW_{3/2} \frac{PT_1 + PT_2}{2}\right] + \frac{F_1}{\alpha}. \quad (4)$$

Here, $C_1 = \rho c \Delta_1 z$ is the bulk heat capacity of the top layer, with ρ and c the density and heat capacity of the ocean and $\Delta_1 z$ the depth of the top layer. The left-hand sides of Eqs. (3) and (4) represent the evolution in time of the temperatures of the nonpolar and polar regions, respectively. The first and second terms on the right-hand sides of these equations represent the air–sea heat exchange, which has the same form as the corresponding terms in Eqs. (1) and (2) but with the opposite sign. The third and fourth terms on the right-hand sides of Eqs. (3) and (4) represent the heat exchange with the underlying layer due to diffusion and vertical advection, respectively. The heat transfer by diffusion is taken to be positive downward and is treated as a Newtonian transfer with heat transfer coefficients $\lambda_{3/2}$ and $\lambda'_{3/2}$ in the nonpolar and polar regions, respectively, where the half-integer subscript indicates the level between layers 1 and 2. The heat transfer by advection is taken to be positive upward, as are the vertical velocities at the base of layer 1 in the nonpolar and polar regions, $W_{3/2}$ and $PW_{3/2}$, respectively. The advected temperature is taken to be the arithmetic mean of the temperatures of layers 1 and 2. The factor $\sigma_{3/2}$ multiplying the third and fourth terms is included to account for the difference in area between the first and second oceanic layers. The last term on the right-hand sides of Eqs. (3) and (4) represents the heat transfer between the nonpolar and polar regions, with F_1 being the meridional heat flux per unit horizontal area of the top layer of the ocean.

The energy equations for the interior and bottom layers of the ocean in the nonpolar and polar regions are

$$C_k \frac{\partial T_k}{\partial t} = \lambda_{k-1/2}(T_{k-1} - T_k) - \rho c W_{k-1/2} \frac{T_{k-1} + T_k}{2} - \sigma_{k+1/2}\left[\lambda_{k+1/2}(T_k - T_{k+1}) - \rho c W_{k+1/2} \frac{T_k + T_{k+1}}{2}\right] - \frac{F_k}{1-\alpha}, \quad k = 2, \cdots, K \quad (5)$$

and

$$C_k \frac{\partial PT_k}{\partial t} = \lambda'_{k-1/2}(PT_{k-1} - PT_k) - \rho c PW_{k-1/2} \frac{PT_{k-1} + PT_k}{2} - \sigma_{k+1/2}\left[\lambda'_{k+1/2}(PT_k - PT_{k+1}) - \rho c PW_{k+1/2} \frac{PT_k + PT_{k+1}}{2}\right] + \frac{F_k}{\alpha}, \quad k = 2, \cdots, K, \quad (6)$$

where $C_k = \rho c \Delta_k z$ is the bulk heat capacity of layer k. The first and second terms on the right-hand sides of Eqs. (5) and (6) represent the heat exchanges with the overlying layer due to diffusion and vertical advection, respectively, while the third and fourth terms represent the corresponding heat exchanges with the underlying layer. These terms are treated as in Eqs. (3) and (4), with $\lambda_{k+1/2}$ and $\lambda'_{k+1/2}$ the Newtonian heat transfer coefficients between layers k and $k+1$ in the nonpolar and polar regions, respectively; $W_{k+1/2}$ and $PW_{k+1/2}$ the respective vertical velocities at the base of layer k in the nonpolar and polar regions; and $\sigma_{k+1/2}$ the ratio of the area of layer $k+1$ to the area of layer k. The final term in Eqs. (5) and (6) represents the transfer of heat between the nonpolar and polar regions of the ocean, with F_k being the meridional heat flux per unit horizontal area of layer k. Because of the boundary conditions for Eqs. (5) and (6); namely,

$$W_{K+1/2} = 0 \quad \text{and} \quad \lambda_{K+1/2} = 0, \quad (7)$$

the latter to satisfy the condition of zero heat flux by diffusion at the ocean bottom, the quantities T_{k+1} and PT_{k+1} appearing in Eqs. (5) and (6) for $k = K$ need not be defined.

For the subsequent analysis it is convenient to eliminate the meridional heat transports F_a and F_k by combining Eqs. (1) and (2), Eqs. (3) and (4), and Eqs. (5) and (6), this after multiplying the odd-numbered equations by $1 - \alpha$ and the even-numbered equations by α. Then defining the global-mean temperatures of the atmosphere and ocean by

$$\bar{T}_a = (1-\alpha)T_a + \alpha PT_a, \quad (8a)$$

and

$$\bar{T}_k = (1-\alpha)T_k + \alpha PT_k, \quad k = 1, \cdots, K, \quad (8b)$$

and using the mass conservation equation for each ocean layer,

$$(1-\alpha)W_{k+1/2} + \alpha PW_{k+1/2} = 0, \quad k = 1, \cdots, K-1, \quad (9)$$

we obtain

$$C_a \frac{\partial \bar{T}_a}{\partial t} = Q - \lambda \bar{T}_a - \sigma_a[A + \lambda_{a,o}(\mu \bar{T}_a - \bar{T}_1)], \quad (10)$$

$$C_1 \frac{\partial \bar{T}_1}{\partial t} = A + \lambda_{a,o}(\mu \bar{T}_a - \bar{T}_1) - \sigma_{3/2}(\lambda_{3/2}G_{3/2} - \rho c W_{3/2}L_{3/2} + \alpha H_{3/2}) \quad (11)$$

and

$$C_k \frac{\partial \bar{T}_k}{\partial t} = (\lambda_{k-1/2}G_{k-1/2} - \rho c W_{k-1/2}L_{k-1/2} + \alpha H_{k-1/2}) - \sigma_{k+1/2}(\lambda_{k+1/2}G_{k+1/2} - \rho c W_{k+1/2}L_{k+1/2} + \alpha H_{k+1/2}), \quad k = 2, \cdots, K, \quad (12)$$

where

$$G_{k-1/2} = \bar{T}_{k-1} - \bar{T}_k, \quad (13)$$

$$L_{k-1/2} = \frac{1}{2}[\bar{T}_{k-1} - \bar{T}_k - (PT_{k-1} + PT_k)], \quad (14)$$

and

$$H_{k-1/2} = (\lambda'_{k-1/2} - \lambda_{k-1/2})(PT_{k-1} - PT_k). \quad (15)$$

Below, we present a method to determine diagnostically from Eqs. (10)–(12) the quantities $\lambda_{k-1/2}$ and $\lambda'_{k-1/2}$ for $k = 2, \cdots, K$; $\lambda_{a,o}$, λ, μ, Q, and A; and F_a and F_k for $k = 1, \cdots, K$. In this method we assume that α and the vertical velocities $W_{k-1/2}$ for $k = 2, \cdots, K$ are known. The prescription of these quantities is described in section 3a.

b. Determination of $\lambda_{k-1/2}$ and $\lambda'_{k-1/2}$ for $k = 2, \cdots, K$

If the time evolutions of T_a, PT_a, T_k, and PT_k are given from the individual $1 \times CO_2$ and $2 \times CO_2$ simulations with the coupled atmosphere–ocean model, Eq. (12) becomes a diagnostic equation in which the values of $\lambda_{k-1/2}$ and $\lambda'_{k-1/2}$ are unknown. If an additional relation between these unknowns is assumed, they can be determined from Eq. (12). Accordingly,

we assume for simplicity that $\lambda'_{k-1/2} = \lambda_{k-1/2}$ for $k = 2, \cdots, K+1$. Thus, $H_{k-1/2} = 0$ for $k = 2, \cdots, K+1$ by Eq. (15), and we can compute $\lambda_{K-1/2}$ from Eq. (12) for $k = K$ written as

$$\lambda_{K-1/2} = \frac{C_K \partial \bar{T}_K / \partial t + \rho c W_{K-1/2} L_{K-1/2}}{G_{K-1/2}}, \quad (16)$$

where the boundary conditions given by Eq. (7) have been used. We can then determine the values of $\lambda_{k-1/2}$ sequentially upward from layer $K-1$ to layer 2 from Eq. (12) written as

$$\lambda_{k-1/2} = \left\{ C_k \frac{\partial \bar{T}_k}{\partial t} + \rho c W_{k-1/2} L_{k-1/2} + \sigma_{k+1/2} [\lambda_{k+1/2} G_{k+1/2} - \rho c W_{k+1/2} L_{k+1/2}] \right\} \Big/ G_{k-1/2}, \quad k = 2, \cdots, K-1. \quad (17)$$

The above analysis for the values of $\lambda_{k-1/2}$ differs from the analysis of Schlesinger et al. (1985) in three ways. First, Schlesinger et al. (1985) assumed that the λ profiles for the $1 \times CO_2$ and $2 \times CO_2$ simulations were identical. Second, because of this assumption it was possible to determine the λ profile from the $2 \times CO_2 - 1 \times CO_2$ temperature differences. However, because the latter were small below the third layer of the model, Schlesinger et al. (1985) were unable to determine the $\lambda_{k-1/2}$ values for layers 4 and 5 of their 6-layer model ($K = 6$). Consequently, to eliminate this shortcoming we determine the λ profiles for each of the $1 \times CO_2$ and $2 \times CO_2$ simulations. Lastly, Schlesinger et al. (1985) integrated in time their equivalent of Eqs. (16) and (17) to eliminate the time derivatives. In the present analysis, instead, we simply evaluate these time derivatives numerically using forward differences.

c. Determination of $\lambda_{a,o}$, λ, μ, A and Q

Equations (10) and (11) can be rewritten diagnostically as

$$Q - \lambda \bar{T}_a - \sigma_a [A + \lambda_{a,o}(\mu \bar{T}_a - \bar{T}_1)] = C_a \frac{\partial \bar{T}_a}{\partial t} \quad (18)$$

and

$$A + \lambda_{a,o}(\mu \bar{T}_a - \bar{T}_1) = C_1 \frac{\partial \bar{T}_1}{\partial t} + \sigma_{3/2}(\lambda_{3/2} G_{3/2} - \rho c W_{3/2} L_{3/2}), \quad (19)$$

where the terms on the right-hand sides are known from the simulation results and the preceding analysis. In obtaining Eq. (19) we have used $H_{3/2} = 0$ obtained from Eq. (15) for $\lambda_{3/2} = \lambda'_{3/2}$.

Equations (18) and (19) can be written for the individual $1 \times CO_2$ and $2 \times CO_2$ simulations, and in the resulting four equations there are ten unknowns; namely, $\lambda_{a,o}$, λ, μ, Q and A for each simulation. Therefore, to close the determination problem we must supply six additional relations. Accordingly, we first assume that λ, $\lambda_{a,o}$ and μ for the $1 \times CO_2$ and $2 \times CO_2$ simulations are the same. Then subtracting Eq. (18) for the $1 \times CO_2$ simulation from Eq. (18) for the $2 \times CO_2$ simulation, and similarly for Eq. (19), we obtain

$$\Delta Q - \lambda \Delta \bar{T}_a - \sigma_a [\Delta A + \lambda_{a,o}(\mu \Delta \bar{T}_a - \Delta \bar{T}_1)] = C_a \frac{\partial \Delta \bar{T}_a}{\partial t} \quad (20)$$

and

$$\Delta A + \lambda_{a,o}(\mu \Delta \bar{T}_a - \Delta \bar{T}_1) = C_1 \frac{\partial \Delta \bar{T}_1}{\partial t} + \sigma_{3/2} \Delta(\lambda_{3/2} G_{3/2} - \rho c W_{3/2} L_{3/2}), \quad (21)$$

where $\Delta\psi = \psi_{2\times CO_2} - \psi_{1\times CO_2}$ for any quantity ψ. Thus, we now have two equations and five unknowns; namely, $\lambda_{a,o}$, λ, μ, ΔQ, and ΔA. Because the latter two quantities respectively represent the changes in the net radiative fluxes at the tropopause and at the earth's surface due to doubling of the CO_2 concentration, we determine them from the results of the $1 \times CO_2$ and $2 \times CO_2$ simulations at their initial time. Lastly, to close the determination problem, we determine μ from its definition given in the Appendix. The unknowns $\lambda_{a,o}$ and λ are then determined from Eqs. (21) and (20), respectively, and the values of A and Q for each simulation are subsequently determined from Eqs. (19) and (18), respectively.

d. Determination of F_a and F_k for $k = 1, \cdots, K$

The meridional heat transports F_k can now be calculated from Eqs. (1), (3), and (5) rewritten as

$$F_a = (1-\alpha)\left\{ -C_a \frac{\partial T_a}{\partial t} + Q - \lambda T_a - \sigma_a [A + \lambda_{a,o}(\mu T_a - T_1)] \right\}, \quad (22)$$

$$F_1 = (1-\alpha)\left\{ -C_1 \frac{\partial T_1}{\partial t} + A + \lambda_{a,o}(\mu T_a - T_1) - \sigma_{3/2}\left[\lambda_{3/2}(T_1 - T_2) - \rho c W_{3/2} \frac{T_1 + T_2}{2} \right] \right\}, \quad (23)$$

and

$$F_k = (1-\alpha)\left\{ -C_k \frac{\partial T_k}{\partial t} + \lambda_{k-1/2}(T_{k-1} - T_k) - \rho c W_{k-1/2} \frac{T_{k-1} + T_k}{2} - \sigma_{k+1/2}\left[\lambda_{k+1/2}(T_k - T_{k+1}) \right. \right.$$

$$- \rho c W_{k+1/2} \frac{T_k + T_{k+1}}{2} \Bigg] \Bigg\},$$

$$k = 2, \cdots, K, \quad (24)$$

or, equivalently, from Eqs. (2), (4), and (6) similarly rewritten.

3. Results

We have presented above a simple atmosphere–ocean model which can be used to represent the results of a coupled atmosphere–ocean general circulation model, the ocean component of which has an arbitrary number of layers K. In the following we will use this simple model with $K = 6$ to represent the results of the OSU coupled atmosphere–ocean GCM, a model in which there are six oceanic layers with thicknesses $\Delta_k z$ as shown in Table 1. However, we shall continue to use the general index K instead of its specific value of 6 to convey the generality of the method.

a. Prescription of α and $W_{k-1/2}$ for $k = 2, \cdots, K$

In the antecedent studies of the time scale of the response of the climate system to increased CO_2 concentrations performed with upwelling–diffusion ocean models, it has generally been assumed that the upwelling velocity W was uniform with depth. The prescribed value of W has ranged from zero in the studies by Hansen et al. (1984), Wigley and Schlesinger (1985), and Schlesinger et al. (1985), to 47.4 m yr^{-1} in the study by Harvey (1986). However, the most commonly prescribed nonzero uniform upwelling velocity has been the value of 4 m yr^{-1} employed, for example, by Hoffert et al. (1980) and Harvey (1986). The use of a uniform upwelling velocity, together with the universal assumption that $\sigma_k = 1$ for all k, greatly simplifies the upwelling–diffusion ocean model. In particular, because there is then no vertical mass flux convergence or divergence for any interior ocean layer in either the nonpolar or polar region, there is no meridional mass flux between the nonpolar and polar regions for the interior ocean layers. Furthermore, because it is implicitly assumed in upwelling–diffusion ocean models that the meridional heat flux is proportional to the meridional mass flux, the meridional heat flux for all interior layers is zero in these models. This is equivalent to assuming that $F_k = 0$ for $k = 2, \cdots, K - 1$ in our model. Because the estimate of the time scale of the response of the climate system to increased CO_2 concentrations may depend on the prescribed vertical velocity profile, we examine below whether the vertical velocities simulated by the coupled atmosphere–ocean general circulation model are uniform with depth.

TABLE 1. Prescribed parameters for the simple atmosphere–ocean model.

Layer k	$\Delta_k z$ (m)	σ_k	C_k (W m^{-2} K^{-1} yr)	$(W_M)_{k-1/2}$ (m yr^{-1}) 1 × CO_2	2 × CO_2
a	—	0.707	0.26	—	—
1	50	0.974	6.64	0.000	0.000
2	200	0.978	26.58	0.726	0.523
3	500	0.973	66.44	1.650	1.355
4	800	0.930	106.30	2.381	1.996
5	1200	0.750	159.45	1.808	1.200
6	1600	0.000	212.60	0.460	0.248
7	—	—	—	0.000	0.000

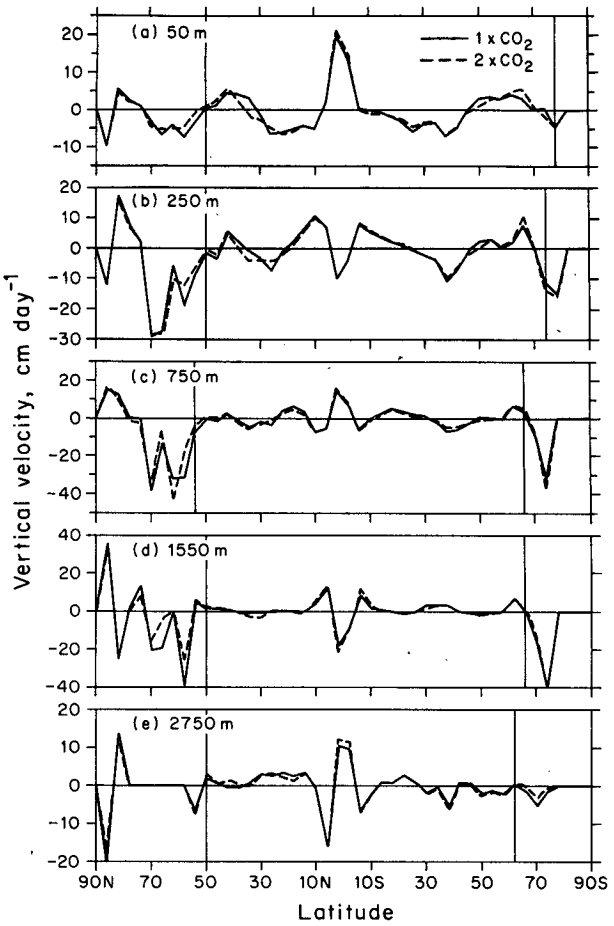

FIG. 2. Latitudinal distribution of the zonally averaged oceanic vertical velocities, $W_{k-1/2}$ for $k = 2, \cdots, 6$, averaged for year 20 of the 1 × CO_2 and 2 × CO_2 simulations by the coupled atmosphere–ocean GCM. The vertical solid lines show the boundaries between the polar and nonpolar regions.

The annually averaged, zonally averaged oceanic vertical velocities $W_{k-1/2}$ for $k = 2, \cdots, K$ are presented in Fig. 2 for year 20 of both the 1 × CO_2 and 2 × CO_2 simulations. This figure shows that the meridional structure of the vertical velocity is not simply that of upwelling in the nonpolar region and downwelling in the corresponding polar region. Instead, the simulated vertical velocity has a richer meridional

structure with features such as equatorial upwelling and subtropical downwelling at the 50-m level ($W_{3/2}$), which are also found in the real ocean. Nevertheless, it can be seen that in high southern latitudes the vertical velocity is downward at each vertical level from about 66°S to the Antarctic continent. In the Northern Hemisphere the vertical velocity is also downward at each vertical level over much of the region poleward of 54°N. Consequently, we initially define the polar region of our model to be the combination of the latitudes 66°S to the Antarctic continent and 54°N–90°N, and the nonpolar region to be the remainder of the ocean from 66°S–54°N. However, the resulting values of α_k decrease with increasing depth (α_k = 0.084, 0.072, 0.061, 0.049, 0.038, 0.014) predominantly because of the broadening of the continents with depth. Because such a depth-dependent value of α leads to a lack of energy conservation in the governing equations of the simple model, we have already assumed a uniform value for α therein. This uniform value of α is obtained as follows. First, a value α^* is chosen as the average of the α_k above. Second, taking into consideration the upwelling profiles, the latitude bounds of each layer are selected to obtain a value α'_k which is very close to α^*. Finally, α is taken as the mass-averaged value of α'_k. This gives α = 0.067. The latitudinal boundaries of the resultant redefined polar and nonpolar regions are shown by the vertical solid lines in Fig. 2. Although we have chosen our single value for α rather carefully, the simple model is not sensitive to the choice of α, as will be shown in section 4.

Having defined the latitudinal extent of the nonpolar and polar regions in the model, we calculate the area-averaged vertical velocities for each of these regions from the data displayed in Fig. 2. The vertical profile of the resultant area-averaged vertical velocities in the nonpolar region is presented in Fig. 3. This figure shows that the vertical velocities are upward at each level. Consequently, the nonpolar region can be identified as the upwelling region. Also, because of the continuity equation (9), the vertical velocities in the polar region are downward at each level. Thus, the polar region can be identified as the downwelling region. The ratio of the magnitudes of the downwelling in the polar region to the magnitude of the upwelling at the same level in the nonpolar region is $(1 - \alpha)/\alpha$ = 14. Figure 3 also shows that the upwelling velocity in the nonpolar region is not uniform with depth for either simulation. Instead, the vertical velocity is zero at the top and bottom of the ocean, as required by the boundary conditions, and attains a maximum magnitude at the 750-m level of 2.4 m yr^{-1} for the 1 × CO_2 simulation and 2.0 m yr^{-1} for the 2 × CO_2 simulation.

The GCM results, therefore, indicate that the assumption of a vertically uniform vertical velocity in the simple model is not valid. However, it is possible that the estimate of the climate time scale may not depend on the prescribed vertical velocity profile because

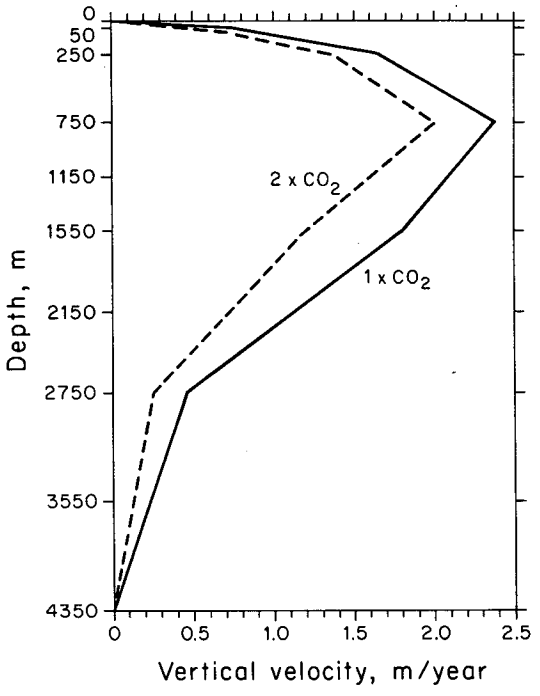

FIG. 3. Vertical profiles of the 1 × CO_2 (solid line) and 2 × CO_2 (dashed line) annual-mean nonpolar vertical velocities for year 20 of the simulations.

of possible compensating effects of other parameters through their dependence on the vertical velocity profile. Therefore, to explore this possibility, we will analyze the GCM results for three prescribed vertical velocity profiles: 1) W_M obtained from the coupled GCM simulations as shown in Fig. 3, with values given in Table 1; 2) W_0 = 0, as employed by box-diffusion ocean models; and 3) W_4 = 4 m yr^{-1}, as employed by most upwelling–diffusion ocean models. For the case of W_4 we assume that α is the same as that for the W_M case; namely, α = 0.067. For the case of W_0, because there is no upwelling or downwelling there is no distinction between the polar and nonpolar regions and α = 0 would seem to be the logical choice. However, the governing equations for the W_0 case show that the results are independent of the choice of α. Consequently, we also employ α = 0.067 for the case of W_0.

In the following three subsections we respectively present the values of $\lambda_{k-1/2}$ for k = 2, · · ·, K; $\lambda_{a,o}$, λ, A and Q; and F_a and F_k for k = 1, · · ·, K. To determine these quantities we have used the values of σ_k and C_k given in Table 1; μ = 0.82, obtained as the average of the values from Eq. (A.21) for January, April, July and October of year 20 of the 1 × CO_2 simulation; ΔQ = 3.92 W m^{-2}, obtained by Schlesinger et al. (1985) at the initial time of the simulations, and ΔA = 1.43 W m^{-2}, also obtained at the initial time. Monthly mean values of the unknown quantities above have been determined over the 20-year simulations

using the monthly mean temperature data from the $1 \times CO_2$ and $2 \times CO_2$ simulations after the annual cycles were removed by a 12 month running-mean filter. In this analysis T_k and PT_k were determined as averages over their respective nonpolar and polar domains and T_a and PT_a were also determined in the same way.

b. *Values of $\lambda_{k-1/2}$ and the corresponding diffusivity $\kappa_{k-1/2}$ for $k = 2, \cdots, K$*

The values of $\lambda_{k-1/2}$ given by Eqs. (16) and (17) are presented in Fig. 4 as a function of time for the $1 \times CO_2$ simulation with the prescribed velocity profiles W_4, W_M, and W_0, each for $\alpha = 0.067$. Figure 4 shows that the values of $\lambda_{k-1/2}$ for each of the W profiles generally increase during the earlier years of the simulations and then reach quasi-constant values. Similar results are obtained for the $2 \times CO_2$ simulation which, therefore, are not shown. Consequently, we average the values of

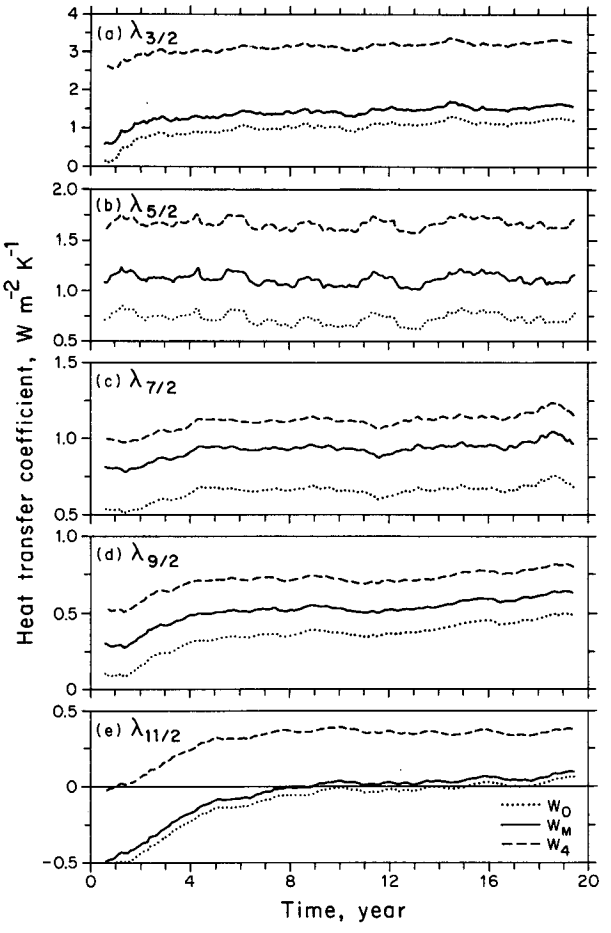

FIG. 4. Temporal evolution of the diffusive heat transfer coefficients $\lambda_{k-1/2}$, $k = 2, \cdots, 6$, for the $1 \times CO_2$ simulation. The dotted, solid, and dashed lines are for W_0, W_M and W_4, respectively, each for $\alpha = 0.067$.

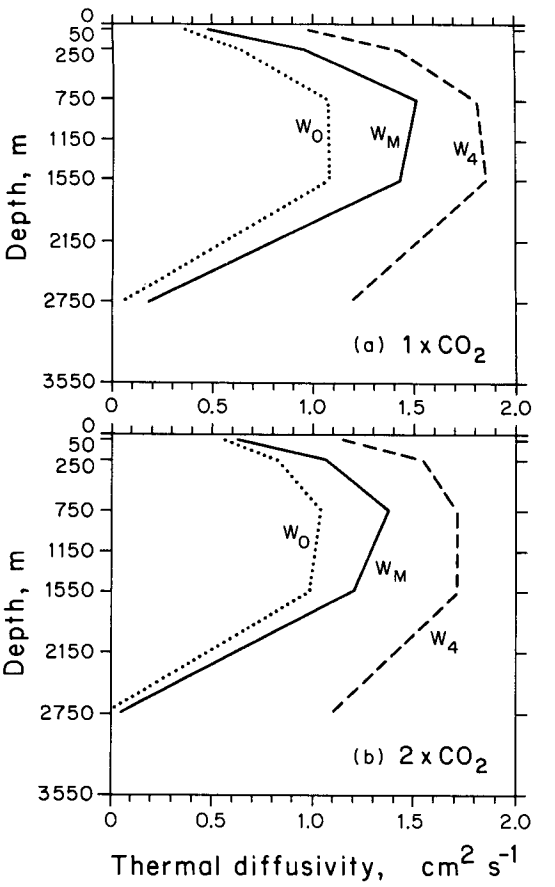

FIG. 5. Vertical profiles of the diffusivity $\kappa_{k-1/2}$, $k = 2, \cdots, 6$, averaged over the last five years of: (a) the $1 \times CO_2$ simulation, and (b) the $2 \times CO_2$ simulation. The dotted, solid, and dashed lines are for W_0, W_M and W_4, respectively, each for $\alpha = 0.067$.

$\lambda_{k-1/2}$ over the last five years of each simulation and convert these values into diffusivities $\kappa_{k-1/2}$ using

$$\kappa_{k-1/2} = \frac{(\Delta_{k-1}z + \Delta_k z)\lambda_{k-1/2}}{2\rho c}. \qquad (25)$$

The vertical profiles of the diffusivities $\kappa_{k-1/2}$ are presented in Fig. 5 for W_4, W_M, and W_0, again each for $\alpha = 0.067$. This figure shows that the values of κ at any depth increase as the prescribed vertical velocity $W(z)$ increases from W_0 to W_M to W_4. This increase in the diffusivities with increasing upwelling velocity is what is required so that the difference between the downward heat transport by diffusion and the upward heat transport by advection remains equal to the net vertical heat transport simulated by the coupled atmosphere–ocean GCM. Figure 5 also shows that κ attains a maximum value at either the 750 or 1550 m level for each of the vertical velocity profiles.

The values of κ obtained here for the W_0 profile are considerably smaller than those obtained by Schlesinger et al. (1985) for the same velocity profile with $\alpha = 0$;

namely, $\kappa_{k-1/2}$ = 3.23, 3.84 and 1.52 cm^2 s^{-1} for k = 2, 3, 4 (50, 250 and 750 m), respectively. To explain the reason for this difference, we write Eq. (12) for the W_0 case with $\alpha = 0$,

$$C_k \frac{\partial \bar{T}_k}{\partial t} = \lambda_{k-1/2}(\bar{T}_{k-1} - \bar{T}_k) - \sigma_{k+1/2}\lambda_{k+1/2}(\bar{T}_k - \bar{T}_{k+1}). \quad (26)$$

Subtracting Eq. (26) for the 1 × CO_2 simulation from Eq. (26) for the 2 × CO_2 simulation gives

$$C_k \frac{\partial \Delta\bar{T}_k}{\partial t} = (\lambda_{k-1/2})_{1\times CO_2}(\Delta\bar{T}_{k-1} - \Delta\bar{T}_k) - \sigma_{k+1/2}(\lambda_{k+1/2})_{1\times CO_2}(\Delta\bar{T}_k - \Delta\bar{T}_{k+1}) + D_k, \quad (27)$$

where

$$D_k = \Delta\lambda_{k-1/2}(\bar{T}_{k-1} - \bar{T}_k)_{2\times CO_2} + \sigma_{k+1/2}\Delta\lambda_{k+1/2}(\bar{T}_k - \bar{T}_{k+1})_{2\times CO_2}. \quad (28)$$

Because Schlesinger et al. (1985) assumed that the λ profiles for the 1 × CO_2 and 2 × CO_2 simulations were identical, they set $D_k = 0$ in Eq. (27). We have repeated our calculation with this assumption and have obtained values very similar to those of Schlesinger et al. (1985) with the small differences predominantly being due to finite differencing the time derivative rather than integrating it as did Schlesinger et al. (1985). Thus, even though the differences in the λ profiles for the 1 × CO_2 and 2 × CO_2 simulations are small as indicated by Fig. 5, D_k is not negligible compared to the other terms in Eq. (27) owing to the size of the multiplicative terms $(T_{k-1} - T_k)_{2\times CO_2}$ and $(T_k - T_{k+1})_{2\times CO_2}$. Consequently, the neglect of D_k in Eq. (27) by Schlesinger et al. (1985) results in their λ and κ values being erroneously large.

The vertically nonuniform profile of $\kappa_{k-1/2}$ obtained in the present analysis, like that of Schlesinger et al. (1985), is in contrast to the vertically uniform value of κ generally assumed in box-diffusion and upwelling–diffusion models, the latter with values ranging from 0.63 cm^2 s^{-1} (Hoffert et al. 1980) to about 2 cm^2 s^{-1} (Hansen et al. 1984). The κ profiles from our analysis generally lie within this range but are smaller than the values of $1.7 \leq \kappa \leq 3.3$ cm^2 s^{-1} determined by Broecker et al. (1980) to be required by a box-diffusion model to reproduce the observed penetration of bomb-produced tritium and ^{14}C into the ocean. Moreover, our values of κ are in agreement with the values of about 0.1–1.3 cm^2 s^{-1} deduced by Kraus (1990) from a presumed dependence of κ on the vertical static stability. However, our κ profiles attain maximum values between 750 and 1550 m while the κ profile of Kraus (1990) monotonically increases with depth. In any case κ in the simple atmosphere–ocean model is an effective diffusivity that encompasses the vertical heat transports by all nonadvective processes. Thus, it may not be very meaningful to compare the κ profile obtained from this simple model with the widely varying estimates of κ based on different observations. This conjecture is supported by the findings of Schlesinger and Jiang (1988) who showed that the nonadvective vertical heat transport in the oceanic component of the coupled atmosphere–ocean GCM is dominated by the convective heat transport, despite the prescribed vertical eddy diffusivity being 1 cm^2 s^{-1} in the ocean GCM.

c. *Values of* $\lambda_{a,o}$, λ, *A and Q*

The values of $\lambda_{a,o}$ and λ obtained respectively from Eqs. (21) and (20), and the values of A and Q for the 1 × CO_2 simulation obtained respectively by Eqs. (19) and (18), are independent of the vertical velocity profiles and the value of α. Figure 6 shows that these quantities rapidly reach their respective equilibrium values about which they oscillate with both intra- and interannual variability. Averaging over the last five years of the 1 × CO_2 and 2 × CO_2 simulations gives the values presented in Table 2. In this table the individual values of $\lambda_{a,o}$ and λ are the same for both the 1 × CO_2 and 2 × CO_2 simulations, this by one of the closure assumptions, and the 2 × CO_2 − 1 × CO_2 differences in

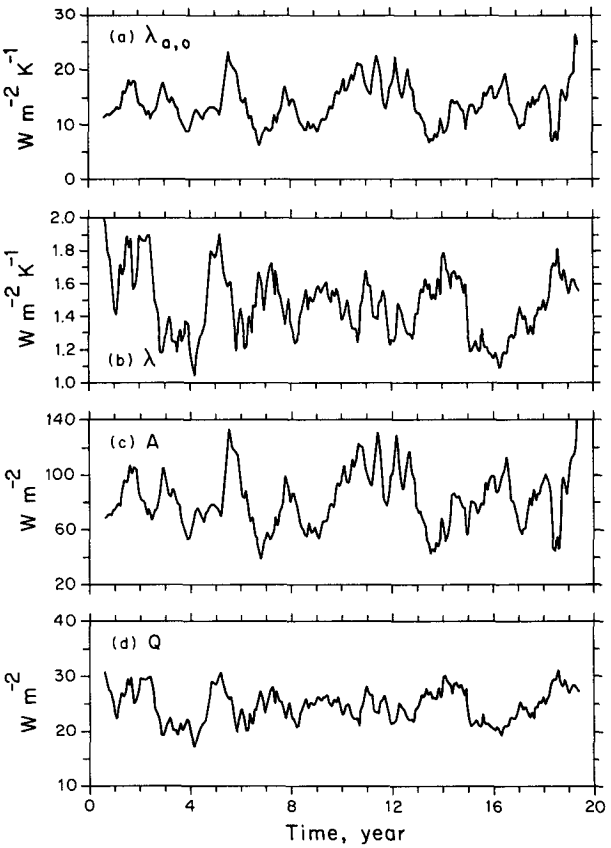

FIG. 6. Temporal evolution of $\lambda_{a,o}$, λ, $A_{1\times CO_2}$ and $Q_{1\times CO_2}$. The results are identical for W_0, W_M and W_4, each for $\alpha = 0.067$.

TABLE 2. Parameters derived from the simple atmosphere-ocean model for the 1 × CO_2 and 2 × CO_2 simulations.

Quantity	1 × CO_2	2 × CO_2
$\lambda_{a,o}$ (W m^{-2} K^{-1})[a]	14.2	14.2
λ (W m^{-2} K^{-1})[a]	1.41	1.41
A (W m^{-2})	84.0	85.4
Q (W m^{-2})	24.7	28.6

[a] The values for 1 × CO_2 and 2 × CO_2 are assumed equal in the analysis.

A and Q are 1.43 and 3.92 Wm^{-2}, this by the given values of ΔA and ΔQ.

The value of $\lambda_{a,o}$ = 14.2 W m^{-2} K^{-1} obtained by the present analysis is in reasonable agreement with the value of $\lambda_{a,o}$ = 16.6 W m^{-2} K^{-1} obtained by Eq. (A.20) in the Appendix. These values are about 80% larger than the value of $\lambda_{a,o}$ = 8.00 W m^{-2} K^{-1} obtained by Schlesinger et al. (1985), but are still smaller than the value of 45 W m^{-2} K^{-1} estimated for the NCAR atmospheric GCM by Dickinson (1981).

The value of λ = 1.41 W m^{-2} K^{-1} obtained by the present analysis is in good agreement with the value of λ = 1.39 W m^{-2} K^{-1} obtained by Schlesinger et al. (1985). In this earlier analysis with a box-diffusion ocean model, the equilibrium warming was given by $\Delta\bar{T} = \Delta\bar{Q}/\lambda$ and was the same for the atmosphere and each oceanic layer. In the present analysis with the generalized upwelling–diffusion ocean model, the equilibrium warming of the atmosphere is again given by $\Delta\bar{T}_a = \Delta Q/\lambda$, but the equilibrium warming of the ocean is no longer equal to this atmospheric warming. In section 4 we will derive expressions from our governing equations for the equilibrium temperature profiles for the 1 × CO_2 and 2 × CO_2 simulations and, thereby, show that the CO_2-induced warming is not vertically uniform when the upwelling velocity is nonzero.

d. *Values of F_a and F_k for k = 1, · · ·, K*

The values of F_a and F_k for k = 1, · · ·, K obtained from Eqs. (22)–(24) for the 1 × CO_2 simulation are presented in Fig. 7 as a function of time for W_4, W_M and W_0. This figure shows that the oceanic meridional heat transports, F_k, depend on the assumed oceanic vertical velocity profile, while the atmospheric meridional heat transport, F_a, does not. In general the meridional heat transports exhibit both intra- and interannual variability superposed on their quasi-stationary equilibrium values. Similar results are obtained for the 2 × CO_2 simulation and, therefore, are not presented. Consequently, we have averaged the meridional heat transports over the last five years of the 1 × CO_2 and 2 × CO_2 simulations, and the resulting vertical profiles are presented in Fig. 8. This figure shows that the meridional heat transports for W_M and W_4 generally are from the nonpolar region to the polar region in the upper three ocean layers, and are from the polar region to the nonpolar region in the lower three ocean layers. For W_0, however, the meridional heat transports at all depths are from the nonpolar to the polar region. Figure 8 also shows that there are small differences in the meridional heat transports between the 1 × CO_2 and 2 × CO_2 simulations.

The agreement between the directions of the meridional heat transport and the meridional mass transport, the latter as determined from the convergence and divergence of the vertical velocity profile is presented in Table 3. This table shows that: 1) for the W_0 and W_4 cases, the meridional mass transport for the interior layers is zero while the corresponding heat transports are nonzero; and 2) for the W_M case, the meridional heat transport for the lowest ocean layer is in the opposite direction from the meridional mass transport. These results indicate that it is impossible to parameterize the meridional heat transport for all the ocean

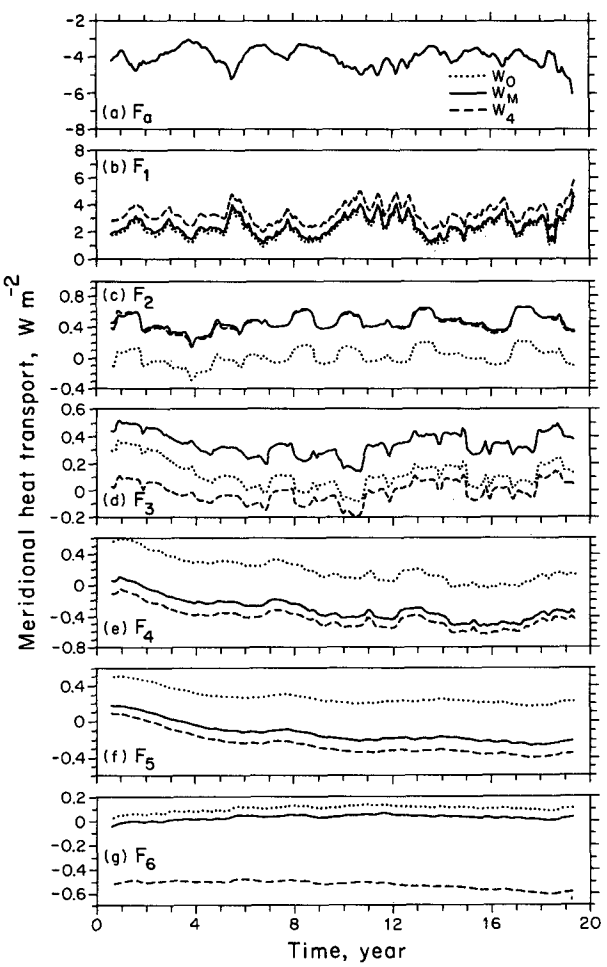

FIG. 7. Temporal evolution of the meridional heat transports in the atmosphere, F_a, and the ocean, F_k, k = 1, · · ·, 6, for the 1 × CO_2 simulation. The dotted, solid, and dashed lines are for W_0, W_M, and W_4, respectively, each for α = 0.067.

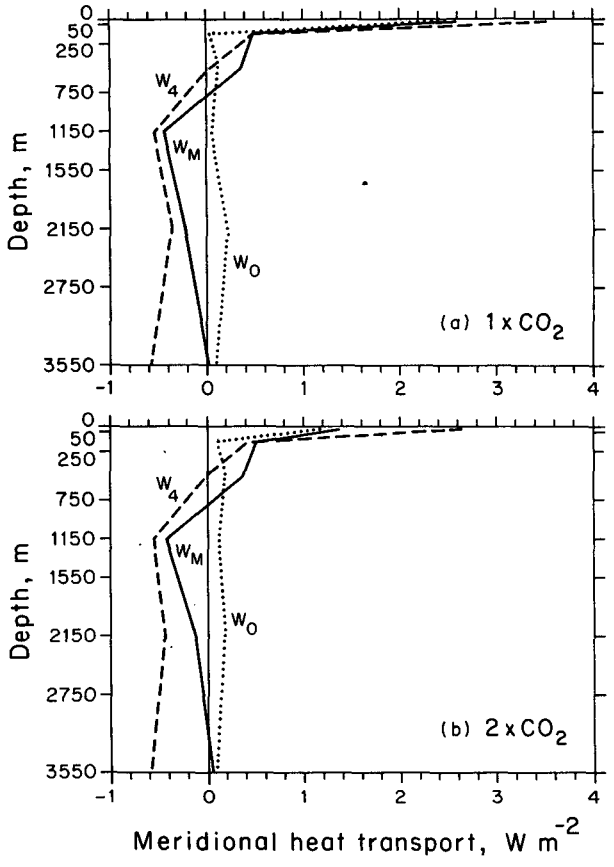

FIG. 8. Vertical profiles of the meridional heat transports in the atmosphere, F_a, and the ocean, F_k, $k = 1, \cdots, 6$, averaged over the last five years of: (a) the $1 \times CO_2$ simulation, and (b) the $2 \times CO_2$ simulation. Positive values represent transports from the nonpolar region to the polar region. The dotted, solid, and dashed lines are for W_0, W_M, and W_4, respectively, each for $\alpha = 0.067$.

layers in terms of the corresponding meridional mass transport.

e. *Closure of the model*

To employ the simple atmosphere–ocean model to represent the behavior of the coupled atmosphere–ocean GCM, we can integrate in time either Eqs. (1)–(6) for the nonpolar and polar temperatures or Eqs. (10)–(12) for the global-mean temperatures. In the former case we must somehow determine the meridional heat fluxes F_a and F_k for all k. In the latter case we must somehow determine the polar temperatures PT_a and PT_k for all k. This is required to evaluate the term $L_{k-1/2}$ in Eqs. (11) and (12) which multiplies the vertical velocity $W_{k-1/2}$. Thus, there is a closure requirement for whichever system of equations is chosen.

The need for closure also occurs in upwelling–diffusion ocean models. Following Hoffert et al. (1980), these models frequently assume that the potential temperature in the polar region, θ_p, is uniform with depth and is given by

$$\theta_p = b + \Pi\theta_m, \tag{29}$$

where θ_m is the potential temperature of the top layer in the nonpolar region, and b and Π are parameters—the latter prescribed to be $0 \leq \Pi \leq 2$. In such upwelling–diffusion models the estimate of the time scale of the response of the climate system to increased CO_2 critically depends upon the value chosen for Π. In particular, the characteristic time scale for the upwelling–diffusion model with $W = 4$ m yr^{-1} for $\Pi = 1$ is longer than the time scale of the box–diffusion model (the upwelling–diffusion model with $W = 0$), but for $\Pi = 0$ is shorter than this time scale (Hoffert et al. 1980; Harvey and Schneider 1985; Schlesinger 1989).

Here we can determine from the results of the coupled atmosphere–ocean GCM simulations whether the above parameterization of the polar temperatures used in upwelling–diffusion models is valid for the coupled atmosphere–ocean GCM. First we examine the assumption that the polar ocean (potential) temperature is uniform in the vertical.

The annually averaged vertical profiles of in situ temperature in the polar region for year 20 of the $1 \times CO_2$ and $2 \times CO_2$ simulations are presented in Fig. 9. This figure shows that the in situ polar temperatures range from 0.8°C for the bottom layer to values between 3.8° and 4.2°C for layer 3 centered at 500 m

TABLE 3. Directions of the meridional heat transport (H) and meridional mass transport (M) for the $1 \times CO_2$ and $2 \times CO_2$ simulations. The symbol + represents a flux from the nonpolar to the polar region, − represents a flux from the polar to the nonpolar region, and 0 means that there is no meridional flux.

	$1 \times CO_2$						$2 \times CO_2$					
	W_0		W_M		W_4		W_0		W_M		W_4	
Layer	M	H	M	H	M	H	M	H	M	H	M	H
1	0	+	+	+	+	+	0	+	+	+	+	+
2	0	+	+	+	0	+	0	+	+	+	0	+
3	0	+	+	+	0	+	0	+	+	+	0	+
4	0	+	−	−	0	−	0	+	−	−	0	−
5	0	+	−	−	0	−	0	+	−	−	0	−
6	0	+	−	+	−	−	0	+	−	+	−	−

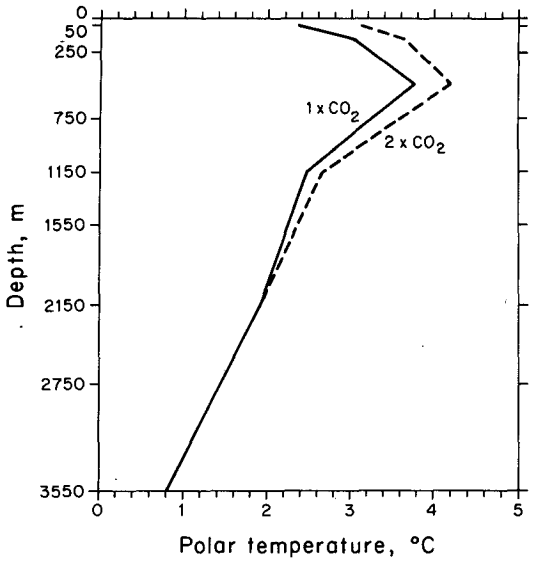

FIG. 9. Vertical profiles of the $1 \times CO_2$ (solid line) and $2 \times CO_2$ (dashed line) annual-mean polar temperatures for year 20 of the simulations.

depth. Taking into consideration the fact that the potential temperature is colder than the in situ temperature at the same depth, with the temperature deficit increasing with depth from about 0.06°C at 1000 m to 0.24°C at 3500 m (Knauss 1978), it can be seen that the potential temperatures are less vertically uniform than the in situ temperatures. Thus, neither the in situ temperature nor the potential temperature in the polar region is uniform with depth.

Because the polar temperatures are not uniform with depth for the coupled atmosphere–ocean GCM we cannot use the closure hypothesis of Hoffert et al. (1980) as given by Eq. (29). However, we can seek a generalization of this closure hypothesis in the form

$$PT_k = A_k + B_k T_1, \quad k = a, 1, \cdots, 6, \quad (30)$$

where A_k and B_k are parameters of a linear regression of the polar temperature for each layer, PT_k, including the atmosphere (subscript a), in terms of the nonpolar temperature of the top layer of the ocean, T_1. The results of such a linear regression using the annual-mean temperatures of both the $1 \times CO_2$ and $2 \times CO_2$ simulations together are presented in Table 4. This table shows that Eq. (30) is a satisfactory closure hypothesis only for the atmosphere and layers 1–3 of the ocean. This result is not particularly surprising due to the lack of vertical uniformity of the polar temperature profile. Therefore, it seems more reasonable to seek a local closure hypothesis for PT_k in terms of the nonpolar temperature for the same layer; that is,

$$PT_k = A_k + B_k T_k, \quad k = a, 1, \cdots, 6. \quad (31)$$

The results of this linear regression, again using the annual-mean temperatures of the $1 \times CO_2$ and $2 \times CO_2$ simulations together, are presented in Fig. 10 and Table 4. From this table it can be seen that Eq. (31) is a satisfactory closure hypothesis for the atmosphere and all the layers of the ocean. Consequently, we adopt Eq. (31) as the closure hypothesis for the simple coupled atmosphere–ocean model.

f. Validation of the model

We can now evaluate the fidelity of the simple model in reproducing the $1 \times CO_2$ and $2 \times CO_2$ simulations of the coupled atmosphere–ocean GCM. To do this we will integrate Eqs. (10)–(12) for the global-mean temperatures over the 20 years of the individual $1 \times CO_2$ and $2 \times CO_2$ simulations beginning from their common initial conditions. In these integrations we will use the time-independent values of α and $W_{k-1/2}$, the time-dependent values of $\lambda_{k-1/2}$, $\lambda_{a,o}$, λ, A and Q determined above, and the closure hypothesis for PT_k in terms of T_k given by Eq. (31). The results of these integrations are presented in Fig. 11 in terms of the evolution of the difference between the $2 \times CO_2$ and $1 \times CO_2$ temperatures, this in comparison with the actual evolution of this temperature difference as simulated by the coupled atmosphere–ocean model. This figure clearly demonstrates that the simple atmosphere–ocean model does give a good representation of the CO_2-induced warming simulated by the coupled atmosphere–ocean model. For the individual $1 \times CO_2$ and $2 \times CO_2$ simulations, the results from the simple atmosphere–ocean model are almost identical to the

TABLE 4. Parameters of the linear regression of the polar temperatures PT_k with T_1 and with T_k. The quantity r_k is the correlation coefficient.

	$PT_k = A_k + B_k T_1$			$PT_k = A_k + B_k T_k$		
Layer k	A_k (°C)	B_k	r_k	A_k (°C)	B_k	r_k
a	−36.769	1.549	0.811	−26.377	1.154	0.799
1	−8.623	0.569	0.884	−8.623	0.569	0.884
2	−4.209	0.381	0.846	−5.503	0.558	0.859
3	−1.663	0.286	0.934	−5.049	0.886	0.871
4	−3.703	0.308	0.727	−6.334	1.729	0.946
5	−1.555	0.167	0.592	−12.253	5.719	0.966
6	−0.008	0.004	0.550	11.554	−7.159	−0.950

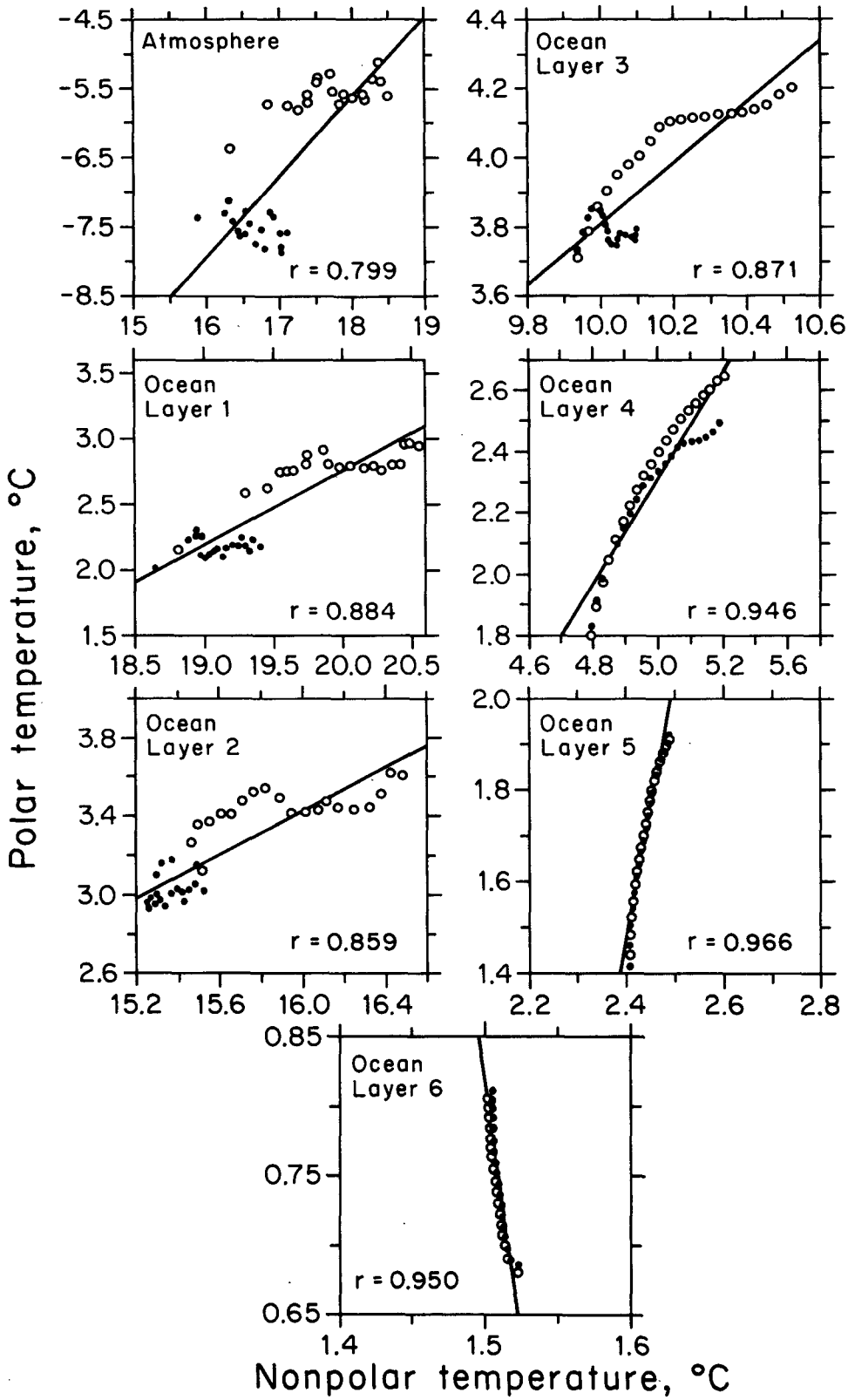

FIG. 10. Scatter plot of the annual-mean polar temperatures PT_k, $k = 1, \cdots, 6$, versus the annual-mean, nonpolar temperature T_k, $k = 1, \cdots, 6$ for the $1 \times CO_2$ (solid circles) and $2 \times CO_2$ (open circles) simulations. The solid lines are least-square fits of the data.

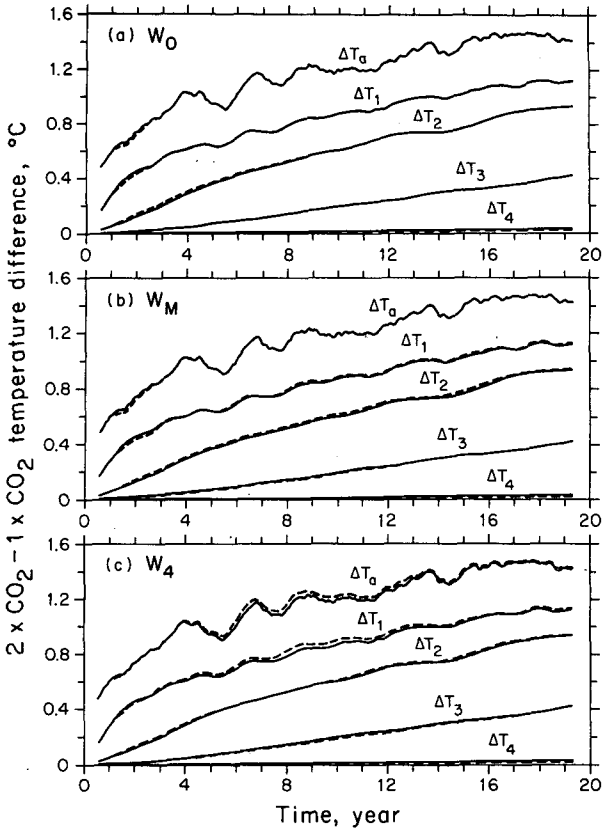

FIG. 11. Time evolutions of the $2 \times CO_2 - 1 \times CO_2$ differences in the annual-mean atmospheric temperature, T_a, and oceanic temperatures, T_k, $k = 1, \cdots, 4$, given by the coupled atmosphere–ocean GCM (solid line) and the simple atmosphere–ocean model, the latter with time-dependent values of $\lambda_{k-1/2}$, $\lambda_{a,o}$, λ, A and Q (dashed line). The three panels show results for (a) W_0, (b) W_M, and (c) W_4.

actual evolutions simulated by the coupled atmosphere–ocean model. Consequently, in the next section we will use the simple atmosphere–ocean model to project the individual $1 \times CO_2$ and $2 \times CO_2$ simulations for a sufficiently long period of time to enable us to estimate the characteric response time of the climate system.

4. Estimation of the time scale of the CO_2-induced warming

To estimate the characteristic time scale of the response of the climate system due to an instantaneous doubling of the CO_2 concentration, we will employ the simple atmosphere–ocean model defined above to extend the length of the 20-year $1 \times CO_2$ and $2 \times CO_2$ simulations obtained by the coupled atmosphere–ocean general circulation model. As in the validation of the simple model we will integrated Eqs. (10)–(12) for the global-mean temperatures using the time-independent values of α and $W_{k-1/2}$ and the closure hypothesis for PT_k in terms of T_k given by Eq. (31). However, in these integrations beyond the 20-year period of the coupled model simulations, we will not be able to use time-dependent values of $\lambda_{k-1/2}$, $\lambda_{a,o}$, λ, A and Q since such time-dependent values are unknown. Consequently, we are forced to use time-independent values of these quantities at least after year 20.

We take the values of $\lambda_{k-1/2}$, $\lambda_{a,o}$, λ, A and Q to be equal to their averages over the last five years of the 20-year coupled GCM simulations, and we use these time-independent values over the entire length of the simple model integrations. Figure 12 presents the results of the first 20 years of these integrations in the same format as Fig. 11. As expected, the simple model with time-independent parameters does not do as well in reproducing the results of the coupled GCM as the same model with time-dependent parameters. This is particularly true during the early part of the 20-year period when the values of the parameters are least like their averaged values over the last five years of the 20-year period (see Fig. 4). Nevertheless, Fig. 12 shows that the simple model with time-independent parameters is capable of reproducing reasonably well the results of the coupled GCM during the later part of the 20-year period.

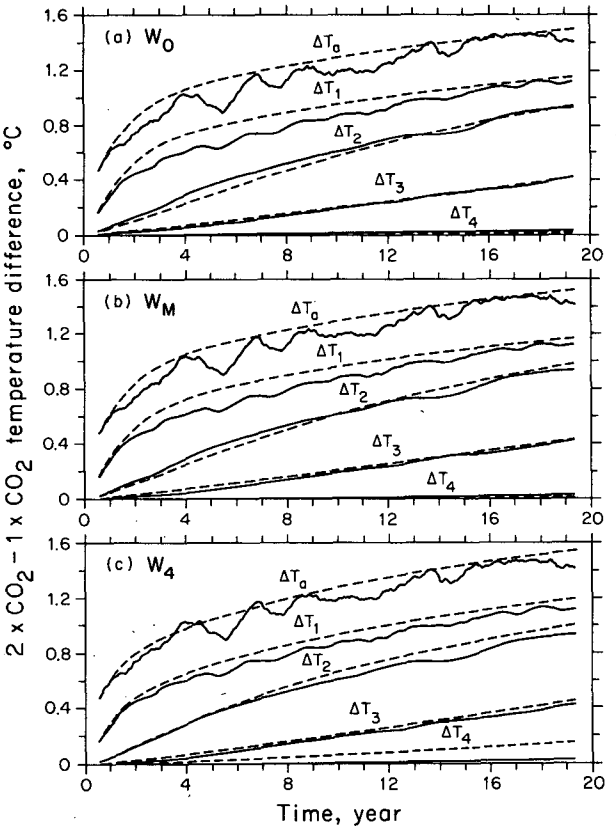

FIG. 12. As in Fig. 11, except the parameters of the simple model are time independent and equal to their averages over the last five years of the 20-year coupled GCM simulations.

To estimate the characteristic response time of the climate system from the simple model extension of the coupled GCM simulations, it is necessary to know the equilibrium temperature change of the model. Knowing the latter allows a normalization of the evolving temperature change so that the time required to reach any fraction of the equilibrium temperature change can be determined. The normalized temperature change of the climate system induced by a doubling of CO_2 is not simply equal to $1 - \exp(-t/\tau_e)$, as would be the case for a mixed-layer ocean that is thermally isolated from the deeper ocean (Schlesinger 1989). Nevertheless, it is useful to define the characteristic response time τ_e in the same way; that is, as the time required to reach $1 - e^{-1} = 0.63$ of the equilibrium temperature change.

The equilibrium temperature profiles for both the $1 \times CO_2$ and $2 \times CO_2$ simulations can easily be obtained by setting the tendency terms in Eqs. (10)–(12) equal to zero and recognizing that the fluxes across the top and bottom of each ocean layer and the atmosphere must be equal to zero, by virtue of the fact that the flux across the bottom of the lowest ocean layer is zero. It can then be shown that the equilibrium temperatures are given by

$$\bar{T}_a = \frac{Q}{\lambda}, \tag{32}$$

$$\bar{T}_1 = \frac{A}{\lambda_{a,o}} + \mu \bar{T}_a, \tag{33}$$

and

$$\bar{T}_k = \frac{\left[\lambda_{k+1/2} - \frac{1}{2}\rho c W_{k+1/2}\left(1 - \frac{1}{\gamma_{k-1} + \alpha}\right)\right]\bar{T}_{k-1} + \frac{1}{2}\rho c W_{k+1/2}\left[\frac{b_{k-1}}{1 + \alpha/\gamma_{k-1}} + \frac{b_k}{1 + \alpha/\gamma_k}\right]}{\lambda_{k+1/2} + \frac{1}{2}\rho c W_{k+1/2}\left(1 - \frac{1}{\gamma_k + \alpha}\right)}, \quad k = 2, \cdots, 6. \tag{34}$$

where

$$\gamma_k = \frac{1 - \alpha}{\Pi_k}. \tag{35}$$

The vertical distribution of the equilibrium temperatures obtained from Eqs. (32)–(34) for the $1 \times CO_2$ simulation are presented in Table 5 for W_0, W_M and W_4, together with the observed temperature distribution. This table shows that although the observed ocean temperatures decrease monotonically with depth, the ocean temperatures are uniform with depth for the W_0 case of zero upwelling. This uniform temperature distribution is evident from Eq. (34) with $W_{k+1/2} = 0$, a well-known result of the box-diffusion model that our model becomes for W_0. Because a uniform temperature distribution is also obtained for the $2 \times CO_2$ simulation the CO_2-induced warming of the ocean is uniform with depth for W_0. However, even in this case of zero upwelling our simple atmosphere–ocean model yields a different warming of the atmosphere and upper ocean layer, as is evident from Eqs. (32) and (33), both of which are independent of the vertical velocities in the ocean. This is in contrast to what was obtained by Schlesinger et al. (1985); namely, that the warming of the atmosphere and upper ocean layer were equal and given by the difference form of Eq. (32), $\Delta\bar{T}_a = \Delta Q/\lambda$. Thus, the criticism of Harvey (1986) that the analysis of Schlesinger et al. (1985) was likely deficient due to the assumption of equal warming of the atmosphere and upper ocean layer has been alleviated by our simple atmosphere-generalized ocean model.

TABLE 5. Global-mean ocean temperature (°C) from observations (Levitus 1982) and the global-mean equilibrium temperature from the simple atmosphere–ocean model for $1 \times CO_2$.

Layer	Depth (m)	Obs	W_0	W_M	W_4
a	—	14.3	17.5	17.5	17.5
1	50	17.5	20.3	20.3	20.3
2	250	14.7	20.3	19.3	17.9
3	500	9.5	20.3	17.4	14.8
4	1150	4.6	20.3	17.2	14.2
5	2150	2.3	20.3	50.0	−89.6
6	3550	1.5	20.3	14.6	−22.2

For $W_{k+1/2} \neq 0$, Eq. (34) shows that the ocean temperature distribution is not uniform with depth. This is corroborated by Table 5, which shows a decreasing temperature from layer 1 through layer 4 for both W_M and W_4. However, the rate at which the temperature decreases with depth is much less than that observed. Furthermore, the changes in temperature in layers 5 and 6 are nonphysical for both W_M and W_4. The likely cause of these unrealistic results below layer 4 of the ocean model is that the values of the parameters $\lambda_{k-1/2}$, $\lambda_{a,o}$, λ, A and Q are not constant in time as a result of the ocean model's not being in equilibrium. Consequently, we should not use our calibrated simple atmosphere–ocean model to project the temperatures of the coupled GCM $1 \times CO_2$ and $2 \times CO_2$ simulations all the way from their 20 year terminus to equilibrium. However, as shown below, our estimates of τ_e are virtually independent of the changes in temperature in layers 5 and 6.

Figure 13 shows the results of using the calibrated simple model to extend the coupled GCM $1 \times CO_2$ and $2 \times CO_2$ simulations from year 20 to year 100, with the differences between these extended simulations being normalized by the equilibrium temperature changes obtained from Eqs. (32)–(34). Because these equilibrium temperature changes for the ocean below layer 3 are likely in error for the reason given above we focus on the temperature changes for the atmosphere and upper ocean layer; these being in any event

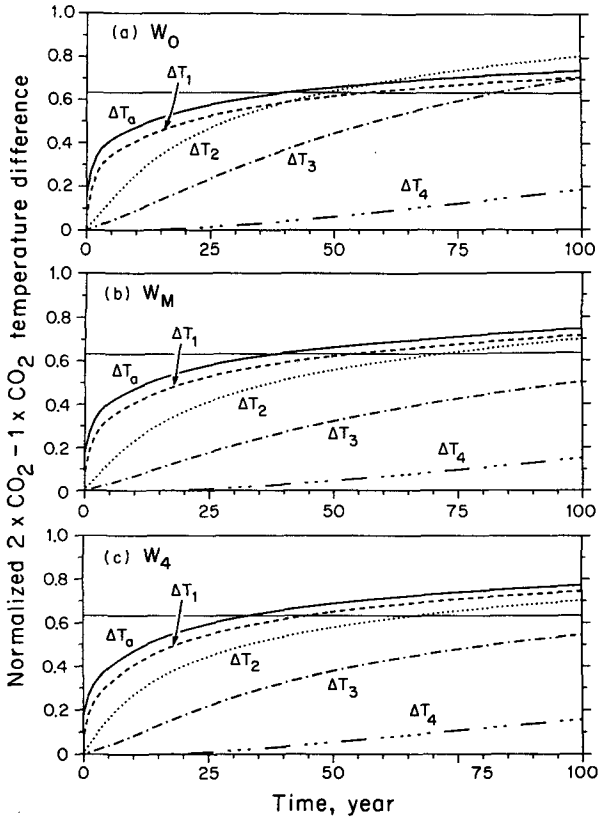

FIG. 13. Time projections of the $2 \times CO_2 - 1 \times CO_2$ differences in the annual-mean atmospheric temperature, T_a, and oceanic temperatures, T_k, $k = 1, \cdots, 4$, normalized by their respective equilibrium temperature change, as given by the simple atmosphere–ocean model with the same time-independent parameters used in Fig. 12. The three panels show results for (a) W_0, (b) W_M, and (c) W_4.

the important temperature changes insofar as the time scale is concerned. The estimated equilibrium temperature changes of the atmosphere and upper ocean layer, given respectively by Eqs. (32) and (33), are $\Delta T_a = 2.78°C$ and $\Delta T_1 = 2.38°C$; the former being virtually identical to the estimate of Schlesinger et al. (1985).

The characteristic response time τ_e, defined as above and determined from the results given in Fig. 13, is presented in Table 6 for the surface air temperature, $\tau_e(\Delta T_a)$, and the temperature of the upper ocean layer, $\tau_e(\Delta T_1)$, for each of the three velocity profiles. This table shows that both values of τ_e decrease as the vertical upwelling increases from zero to W_M to W_4, thus supporting the conclusion of Harvey (1986). However, the decrease in $\tau_e(\Delta T_a)$ and $\tau_e(\Delta T_1)$ from W_0 to our best estimate of the vertical velocity, W_M, is not more than four years. These estimates are reduced somewhat if the upwelling velocity is taken to be W_4, the usual value assumed in upwelling-diffusion ocean models.

We have further tested the robustness of our τ_e estimates as follows. First, we have used the vertical velocity profile suggested by Hoffert (1989, personal communication), namely, $W_H = W_4(T_s - T)/(T_s - T_b)$, where T_s and T_b are the surface and bottom temperatures of the ocean, respectively. The results are $\tau_e(\Delta T_a) = 37$ and $\tau_e(\Delta T_1) = 52$ years, which are midway between the values for our W_M and W_4 profiles. Second, we have changed the value of α from 0.067 to its minimum and maximum values over all the ocean layers, 0.014 and 0.084. This changed $\tau_e(\Delta T_a)$ by one year for W_0 and W_4, and by less than one year for W_M, and changed $\tau_e(\Delta T_1)$ by two years for W_0, and by less than one year for W_4 and W_M. Finally, we have checked the dependence of our τ_e estimates on the changes in temperature in layers 5 and 6. To do this we have changed the values of $\lambda_{9/2}$ and $\lambda_{11/2}$, first to be zero and second to be ten times larger than the values obtained in our analysis, both of which changed $\tau_e(\Delta T_a)$ and $\tau_e(\Delta T_1)$ by one year or less.

From these results we conclude that the estimates of $\tau_e(\Delta T_a)$ and $\tau_e(\Delta T_1)$ obtained by Schlesinger et al. (1985) are essentially correct and, therefore, that the characteristic response time of the climate system to a CO_2 doubling is between 40 and 60 years. Of course this conclusion is based on our representation by the simple atmosphere–ocean model of the $1 \times CO_2$ and $2 \times CO_2$ simulations by only a single atmosphere–ocean GCM. Further, confidence in the τ_e estimates can be obtained by performing similar analyses of the transient simulations by other atmosphere–ocean GCMs.

5. Summary

A simple atmosphere–generalized ocean model, consisting of a zonally averaged energy-balance climate model and a zonally averaged multilayer ocean model has been developed. In this simple model the high latitudes of both hemispheres are combined into a single polar region and the low and middle latitudes are combined into a single nonpolar region. The atmosphere is treated as a single layer and the ocean is subdivided vertically into an arbitrary number of layers. The nonpolar and polar regions of the atmosphere and each ocean layer occupy depth-independent fractions of their horizontal areas, the latter of which vary in the vertical. The simple model includes the meridional transport of heat between the nonpolar and polar regions for both the atmosphere and each ocean layer.

TABLE 6. Characteristic response time τ_e in years given by the simple atmosphere–ocean model for the atmospheric temperature change (ΔT_a) and the upper ocean layer temperature change (ΔT_1).

Vertical velocity	$\tau_e(\Delta T_a)$	$\tau_e(\Delta T_1)$
W_0	41	57
W_M	39	54
W_4	34	45

The ocean model includes the vertical advective heat transfer by the vertical velocity, the latter of which is prescribed and can vary with depth in both the polar and nonpolar regions. The nonadvective vertical heat transfer within the ocean, the heat transfer between the ocean and the atmosphere, and the heat transfer between the earth and space are each represented as a sum of a temperature-independent part and a temperature-dependent part, as obtained by a linearization about a reference state.

We have used the simple model with six ocean layers to represent the results of the OSU coupled atmosphere/6-layer ocean GCM. In this representation we have made three different assumptions about the vertical velocity profile in the nonpolar region: 1) W_M obtained directly from the coupled GCM simulations, 2) $W_0 = 0$, as employed by box–diffusion ocean models, and 3) $W_4 = 4$ m yr^{-1}, as employed by most upwelling–diffusion ocean models. For each of these profiles the corresponding vertical velocity profile in the polar region is obtained from the continuity equation.

The results of the representation show that the values of the diffusivities for heat (κ) at any depth in the ocean increase as the prescribed vertical velocity increases from W_0 to W_M to W_4. The values of κ obtained here for the W_0 profile are considerably smaller than those obtained by Schlesinger et al. (1985) because of their erroneous assumption that the κ profiles for the $1 \times CO_2$ and $2 \times CO_2$ simulations were identical. The values of the ocean–atmosphere heat transfer coefficient and the climate sensitivity parameter (λ) are found to be independent of the prescribed vertical velocity profile. The value of $\lambda = 1.41$ W m^{-2} K^{-1} obtained here is in good agreement with the value of $\lambda = 1.39$ W m^{-2} K^{-1} obtrained by Schlesinger et al. (1985). The values of the oceanic meridional heat transports (F_k) depend on the assumed oceanic vertical velocity profile while the atmospheric meridional heat transport (F_a) does not. The meridional heat transports for W_M and W_4 generally are from the nonpolar region to the polar region in the upper three ocean layers and are from the polar region to the nonpolar region in the lower three ocean layers. For W_0, however, the meridional heat transports at all depths are from the nonpolar to the polar region.

To employ the simple atmosphere–ocean model to project the response of the coupled atmosphere–ocean GCM beyond the 20-year period of its simulations, we have parameterized the polar temperature for each layer in terms of the nonpolar temperature for the same layer. The fidelity of the simple model was then ascertained using the time-dependent values of its parameters. It is found that the results from the simple atmosphere–ocean model are almost identical to the actual $1 \times CO_2$ and $2 \times CO_2$ evolutions simulated by the coupled atmosphere–ocean model.

To estimate the characteristic time scale of the response of the climate system due to a doubling of the CO_2 concentration, we have employed the simple atmosphere–ocean model to extend the length of the 20-year $1 \times CO_2$ and $2 \times CO_2$ coupled GCM simulations using time-independent values of the simple model parameters taken equal to their averages over the last five years of the 20-year simulations. As expected, the simple model with time-independent parameters does not do as well in reproducing the results of the coupled GCM as the same model with time-dependent parameters. Nevertheless, the simple model with time-independent parameters is capable of reproducing reasonably well the results of the coupled GCM during the later part of the 20-year period.

To estimate the characteristic response time of the climate system from the simple model extension of the coupled GCM simulations, it is also necessary to know the equilibrium temperature change of the model. These estimated equilibrium temperature changes for the atmosphere (ΔT_a) and upper ocean layer (ΔT_1) are 2.78°C and 2.38°C, respectively, the former being virtually identical to the estimate of Schlesinger et al. (1985).

The characteristic response time τ_e, defined as the time required to reach 63% of the equilibrium response for each layer, decreases as the vertical upwelling increases from W_0 to W_M to W_4, thus, supporting the conclusion of Harvey (1986). However, the decrease in $\tau_e(\Delta T_a)$ and $\tau_e(\Delta T_1)$ from W_0 to our best estimate of the vertical velocity, W_M, is not more than four years. From this we conclude that the estimates of $\tau_e(\Delta T_a)$ and $\tau_e(\Delta T_1)$ obtained by Schlesinger et al. (1985) are essentially correct and, therefore, that the characteristic response time of the climate system to a CO_2 doubling is between 40 and 60 years.

Acknowledgments. We thank D. Vickers for his programming assistance. We also thank D. Harvey, M. MacCracken, M. Hoffert and an anonymous reviewer for their constructive comments on the manuscript. Acknowledgment is made to the National Center for Atmospheric Research, which is sponsored by the National Science Foundation, for the NCAR computing time used in this research. This research was supported by the National Science Foundation and the Carbon Dioxide Research Program, Office of Health and Environmental Research of the Department of Energy under Grant ATM-8712033.

APPENDIX

Derivation of the Linearized Heat Flux Expressions

The energy-balance equation for an atmospheric column can be written as

$$C_a \frac{\partial T_a}{\partial t} = S_a + L_S - L_T + H_S + H_L, \quad \text{(A.1)}$$

where C_a is the heat capacity of the atmosphere with temperature T_a, S_a is the solar radiation absorbed by

the atmosphere, L_S and L_T are the net upward longwave radiation fluxes at the earth's surface and top of the atmosphere, respectively, and H_S and H_L are the sensible and latent heat fluxes, respectively, both taken as positive from the surface into the atmosphere. Similarly, the energy equation for the top layer of an oceanic column can be written as

$$C_1 \frac{\partial T_1}{\partial t} = S_S - L_S - H_S - H_L + H_B, \quad \text{(A.2)}$$

where C_1 is the heat capacity of the upper oceanic layer with temperature T_1, S_S is the solar radiation absorbed by the layer, and H_B is the heat flux from the underlying layer.

The net upward longwave radiation at the earth's surface is given by

$$L_S = \sigma {T_1}^4 - \epsilon_a \sigma {T_a}^4, \quad \text{(A.3)}$$

where σ is the Stefan-Boltzmann constant and ϵ_a is an effective emissivity for the downward longwave radiation at the earth's surface. Linearizing Eq. (A.3) about a reference temperature T_{ref} gives

$$L_S = A_1 + B_1(T_1 - \epsilon_a T_a) \quad \text{(A.4)}$$

where

$$A_1 = -3(1 - \epsilon_a)\sigma T_{\text{ref}}^4 \quad \text{(A.5)}$$

and

$$B_1 = 4\sigma T_{\text{ref}}^3. \quad \text{(A.6)}$$

Similarly, the net upward longwave radiation flux at the top of the atmosphere can be approximated as

$$L_T = \epsilon'_a \sigma {T_a}^4 = A_2 + B_2 T_a, \quad \text{(A.7)}$$

where

$$A_2 = -3\epsilon'_a \sigma T_{\text{ref}}^4, \quad \text{(A.8)}$$

and

$$B_2 = 4\epsilon'_a \sigma T_{\text{ref}}^3, \quad \text{(A.9)}$$

and ϵ'_a is an effective emissivity for the upward longwave radiation at the top of the atmosphere.

The sensible and latent heat fluxes are given by

$$H_S = C_S(T_1 - T_a) \quad \text{(A.10)}$$

and

$$H_L = C_L[q^*(T_1) - \text{RH}q^*(T_a)], \quad \text{(A.11)}$$

where C_S and C_L are heat transfer coefficients, $q^*(T_1)$ and $q^*(T_a)$ are the saturated water vapor mixing ratios for the ocean and atmosphere, respectively, and RH is the relative humidity of the atmosphere. Assuming the latter to be constant, Eq. (A.11) can be linearized about T_{ref} to give

$$H_L = A_3 + B_3(T_1 - \text{RH}T_a), \quad \text{(A.12)}$$

where

$$A_3 = C_L\left[(1 - \text{RH})q^*(T_{\text{ref}}) - \left(\frac{\partial q^*}{\partial T}\right)_{T_{\text{ref}}}(1 - \text{RH})T_{\text{ref}}\right] \quad \text{(A.13)}$$

and

$$B_3 = C_L\left(\frac{\partial q^*}{\partial T}\right)_{T_{\text{ref}}}. \quad \text{(A.14)}$$

Substituting Eqs. (A.4), (A.7), (A.10) and (A.12) into Eqs. (A.1) and (A.2) yields

$$C_a \frac{\partial T_a}{\partial t} = Q - \lambda T_a - [A + \lambda_{a,o}(\mu T_a - T_1)] \quad \text{(A.15)}$$

and

$$C_1 \frac{\partial T_1}{\partial t} = A + \lambda_{a,o}(\mu T_a - T_1) + H_B, \quad \text{(A.16)}$$

where

$$Q = S_a + S_S - A_2 \quad \text{(A.17)}$$

is the temperature-independent part of the radiative heat flux at the top of the atmosphere;

$$A = S_S - A_1 - A_3 \quad \text{(A.18)}$$

is the temperature-independent part of heat flux at the sea surface;

$$\lambda = B_2 \quad \text{(A.19)}$$

is a climate sensitivity parameter;

$$\lambda_{a,o} = B_1 + C_S + B_3 \quad \text{(A.20)}$$

is an atmosphere–ocean heat transfer parameter; and

$$\mu = \frac{B_1\epsilon_a + C_S + B_3\,\text{RH}}{B_1 + C_S + B_3} \quad \text{(A.21)}$$

is a parameter that results because ϵ_a and RH may be different from unity.

The values of $\lambda_{a,o}$, λ, A and Q are estimated from the $1 \times CO_2$ and $2 \times CO_2$ simulations as described in the text. For this purpose it is necessary to prescribe the values of C_a, C_1, and μ. For the latter, from Eqs. (A.21), (A.6) and (A.14) it is necessary to prescribe the values of σ, ϵ_a, C_S, C_L, $(\partial q^*/\partial T)_{T_{\text{ref}}}$, and RH. The quantities C_S and C_L are calculated as in the atmospheric GCM:

$$C_S = \rho_a c_p C_D V'_s \quad \text{(A.22)}$$

and

$$C_L = \rho_a L C_D V'_s \beta \quad \text{(A.23)}$$

where ρ_a is the surface air density, c_p is the specific heat at constant pressure, V'_s is the effective surface wind

TABLE A.1. Values of C_S, C_L and the other prescribed quantities determined from the history data of the 1 × CO_2 and 2 × CO_2 simulations.

T_{ref} (K)	C_S (W m^{-2} K^{-1})	C_L (W m^{-2})	$(\partial q^*/\partial T)_{T_{ref}}$ (K^{-1})	RH	ϵ_a
287.1	4.41	8167.0	6.62×10^{-4}	0.665	0.832

speed, C_D is the drag coefficient, and β is the ratio of the actual evapotransporation to the potential evapotransporation (Ghan et al. 1982). The values of C_S, C_L and the other prescribed quantities were determined from the history data of the 1 × CO_2 and 2 × CO_2 simulations and are presented in Table A.1. The resultant value of μ is 0.82.

REFERENCES

Broecker, W. S., T.-H. Peng and R. Engh, 1980: Modeling the carbon system. *Radiocarbon,* **22,** 565–598.

Bryan, K., and M. J. Spelman, 1985: The ocean's response to a CO_2-induced warming. *J. Geophys. Res.,* **90,** 11 679–11 688.

——, F. G. Komro, S. Manabe and M. J. Spelman, 1982: Transient climate response to increasing atmospheric carbon dioxide. *Science,* **215,** 56–58.

——, —— and C. Rooth, 1984: The ocean's transient response to global surface anomalies. *Climate Processes and Climate Sensitivity, Geophys. Monogr. Ser.,* No. 29, Amer. Geophys. Union, 29–38.

Dickinson, R. E., 1981: Convergence rate and stability of ocean–atmosphere coupling schemes with a zero-dimensional climate model. *J. Atmos. Sci.,* **38,** 2112–2120.

Ghan, S. J., J. W. Lingaas, M. E. Schlesinger, R. L. Mobley and W. L. Gates, 1982: A documentation of the OSU two-level atmospheric general circulation model. Report No. 35, Climatic Research Institute, Oregon State University, Corvallis, 395 pp.

Hansen, J., and S. Lebedeff, 1987: Global trends of measured surface air temperature. *J. Geophys. Res.,* **92,** 13 345–13 372.

——, and S. Lebedeff, 1988: Global surface air temperatures: Update through 1987. *Geophys. Res. Lett.,* **15,** 323–326.

——, A. Lacis, D. Rind, G. Russell, P. Stone, I. Fung, R. Ruedy and J. Lerner, 1984: Climate sensitivity: Analysis of feedback mechanisms. *Climate Processes and Climate Sensitivity, Geophys. Monogr. Ser.,* No. 29, Amer. Geophys. Union, 130–163.

Harvey, L. D. D., 1986: Effect of ocean mixing on the transient climate response to a CO_2 increase: analysis of recent model results. *J. Geophys. Res.,* **91,** 2709–2718.

——, and S. H. Schneider, 1985: Transient climate response to external forcing on 10^0–10^4 year time scales. Part 1: Experiments with globally averaged, coupled, atmosphere and ocean energy-balance models. *J. Geophys. Res.,* **90,** 2191–2205.

Hoffert, M. I., A. J. Callegari and C.-T. Hsieh, 1980: The role of deep sea heat storage in the secular response to climate forcing. *J. Geophys. Res.,* **85,** 6667–6679.

Jones, P. D., T. M. L. Wigley and P. B. Wright, 1986: Global temperature-variations between 1861 and 1984. *Nature,* **322,** 430–434.

Knauss, J. A., 1978: *Introduction to Physical Oceanography.* Prentice-Hall, 338 pp.

Kraus, E. B., 1990: Diapycnal Mixing. *Climate-Ocean Interaction,* M. E. Schlesinger, Ed., Kluwer, 269–293.

Levitus, S., 1982: Climatological Atlas of the World Ocean. NOAA Professional Paper No. 13. U.S. Government Printing Office, 173 pp.

Schlesinger, M. E., 1989: Model Projections of the Climatic Changes Induced by Increased Atmospheric CO_2. *Climate and the Geo-Sciences: A Challenge for Science and Society in the 21st Century.* A. Berger, S. Schneider and J. Cl. Duplessy, Eds., Kluwer, 375–415.

——, and X.-J. Jiang, 1988: The transport of CO_2-induced warming into the ocean: an analysis of simulations by the OSU coupled atmosphere–ocean general circulation model. *Climate Dynamics,* **3,** 1–17.

——, W. L. Gates and Y.-J. Han, 1985: The role of the ocean in CO_2-induced climate warming: preliminary results from the OSU coupled atmosphere–ocean GCM. *Coupled Ocean–Atmosphere Models,* J. C. J. Nihoul, Ed., Elsevier, 447–478.

Wigley, T. M. L., and M. E. Schlesinger, 1985: Analytical solution for the effect of increasing CO_2 on global mean temperature. *Nature,* **315,** 649–652.